Dimension-matched Zinc Phthalocyanine/$BiVO_4$ ultrathin nanocomposites for CO_2 Reduction as Efficient Wide-Visible-Light-Driven Photocatalysts via a Cascade Charge Transfer

Ji Bian,[a,b] Jiannan Feng,[a] Ziqing Zhang,[a] Zhijun Li,[a] Yuhang Zhang,[a] Yadi Liu,[c] Sharafat Ali,[a] Yang Qu,[a] Linlu Bai,[a] Jijia Xie,[d] Dongyan Tang,[b] Xin Li,[b] Fuquan Bai,*[c] Junwang Tang,*[d] and Liqiang Jing*[a]

Abstract: Herein, a novel strategy of cascade charge transfer was realised by a H-bond linked zinc phthalocyanine/$BiVO_4$ nanosheet (ZnPc/BVNS) composite, which subsequently works as an efficient wide-visible-light-driven photocatalyst for converting CO_2 to CO and CH_4, proved by both products analysis and ^{13}C isotopic measurement. The optimised ZnPc/BVNS nanocomposite exhibits ~16-fold enhancement in the quantum efficiency compared with the reported $BiVO_4$ nanoparticles at the excitation of 520 nm with an assistance of 660 nm photons. Both experimental and theoretical results verify the exceptional activities are attributed to the rapid charge separation via a novel cascade Z-scheme charge transfer mechanism formed by the dimension-matched ultrathin (~8 nm) heterojunction nanostructure. Moreover, it is evidenced that the central Zn^{2+} in ZnPc could accept the excited electrons from the ligand and then provide a catalytic function for CO_2 reduction. Impressively, this Z-scheme is also feasible to other MPc like FePc and CoPc together with BVNS.

Conversion of CO_2 into valuable fuels through photocatalytic technique is one promising approach to tackle both energy crisis and the related environmental problems.[1-2] $BiVO_4$ as a promising photocatalyst has attracted a great deal of attention owing to its environmental friendliness, chemical stability and narrow bandgap alignment.[3-5] However its excellent oxygen evolution performance does not make it a good candidate for photocatalytic CO_2 reduction due to its low reduction potential. In addition the photocatalytic activity of $BiVO_4$ is also unsatisfactory due to the sluggish charge separation, the limited visible-light utilization and the low efficiency of charge-induced reactions.[6-7]

Generally speaking, the granular morphology of $BiVO_4$ is one of the reasons for its poor charge separation. With emerging of two-dimensional (2D) materials, ultrathin sheet-like $BiVO_4$ is highly desired on account of the minimized diffusion distance and depressed electron-hole recombination.[8] Nevertheless, it was difficult to synthesis $BiVO_4$ nanosheets (BVNS) due to the lacking of intrinsic driving force for anisotropic growth. Recently, Xie's group reported an ultrathin nanostructured $BiVO_4$ by a cetyltrimethylammonium bromide (CTAB)-induced self-assembly method, which provided a feasible route for such morphology fabrication.[9]

Considering sluggish charge separation of $BiVO_4$, we introduced TiO_2 to generate a solid junction in previous work to help electron transfer from $BiVO_4$ to TiO_2, thus prolonging the lifetimes of visible-light induced photoelectrons. [10-11] However, it is not effective for the electrons transfer due to the unmatched energy levels and for the long wavelength visible-light absorption because of its coupled wide-bandgap semiconductors.

Natural photosynthesis demonstrates a Z-scheme photocatalytic system with a step-wise charge-transfer pathway, which is different from the widely used solid junction [11] and can't only favor the photogenerated charge separation but also maintain the excellent redox capacity of two constituent semiconductors.[12-13] A few studies focused on the typical Z-scheme g-C_3N_4/$BiVO_4$ systems.[14-15] However, it is hard to further extend the absorption range since the optical absorption band of g-C_3N_4 is much wider than that of $BiVO_4$. Fortunately, metal phthalocyanines (MPc) are analogous to light-harvester chlorophyll with porphyrin ring, and its conjugated macrocycle structure is much favorable to build a dimension-matched interface with 2D-$BiVO_4$. These inspired us to select MPc to construct a wide-visible-light responsive artificial Z-scheme system with BVNS, owing to their characteristic visible/near-infrared selective absorption regions and the matched energy band alignments (the HOMO energy levels of MPc are close to the CB of $BiVO_4$).[16-17] Expectedly, it would both extend the visible-light absorption and greatly enhance the charge separation.

Zinc phthalocyanine (ZnPc) has attracted much attention as a member of MPc family, and the majority of the studies focus on sensitization for pollutant degradation, hydrogen production and solar cells,[18-19] little work was devoted to the Z-scheme systems for CO_2 conversion. Notably, a number of works has regarded ZnPc as an entirety, little attention was put to the central metal unit. According to the Z-scheme process, if the excited electrons at the ligand further transfer to the coordinated central metal unit, it would potentially make ZnPc possess a catalytic function to CO_2 conversion. Moreover, how to achieve controllable dispersion of ZnPc on a semicondutor is the key to construct a high-quality Z-scheme and expose more active sites. Herein, we report a facile assembly strategy to fabricate dimension-matched ZnPc/$BiVO_4$ nanocomposites with ultrathin structure as efficient photocatalysts for CO_2 conversion based on a novel Z-scheme

[a] J. Bian, J. N. Feng, Z. Q. Zhang, Z. J. Li, Y. H. Zhang, S. Ali, Y. Qu, L. L. Bai, Prof. L. Q. Jing
Department Key Laboratory of Functional Inorganic Materials Chemistry (Ministry of Education), School of Chemistry and Materials Science, International Joint Research Center and Lab for Catalytic Technology
Heilongjiang University, Harbin 150080, P. R. China.
E-mail: jinglq@hlju.edu.cn
[b] Prof. D. Y. Tang, Prof. X. Li
School of Chemistry and Chemical Engineering
Harbin Institute of Technology, Harbin 150001, P. R. China.
E-mail: dytang@hit.edu.cn, lixin@hit.edu.cn
[c] Y. D. Liu, Prof. F. Q. Bai
International Joint Research Laboratory of Nano-Micro Architecture Chemistry, Institute of Theoretical Chemistry
Jilin University, Changchun 130021, P. R. China.
E-mail: baifq@jlu.edu.cn
[d] J. Xie, Prof. J. Tang
Department of Chemical Engineering
University College London, Torrington Place, London WC1E 7JE, UK.
E-mail: Junwang.tang@ucl.ac.uk

charge transfer mechanism. In the one-pot assembly process, hydroxylated BVNS were first formed, followed by the surface hydroxyl group-induced assembly for polymeric ZnPc to uniformly dispersed on the BVNS (Scheme 1).

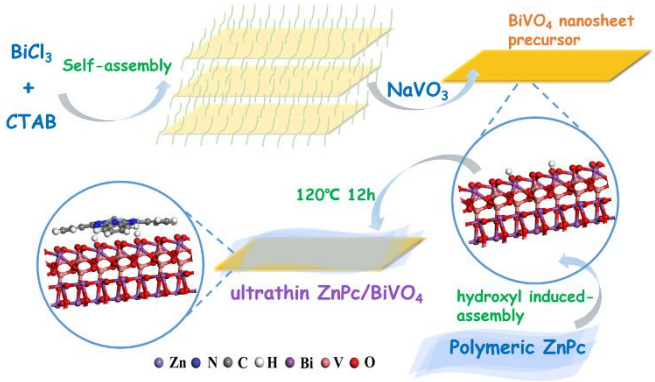

Scheme 1. Schematic pathway of ultrathin ZnPc/BVNS heterojunction.

The obtained BVNS are indexed to the monoclinic phase (JCPDS no.14-0688), as shown in Figure S1. The relative intensity ratio of the (200) to the (121) peak is 2.4 times higher compared with that of previously reported $BiVO_4$ nanoparticles (BVNP) obtained by a co-precipitation method,[11] implying its selective growth along (200) crystal plane for BVNS. No noticeable peaks from ZnPc can be observed in the patterns of nanocomposites due to its tiny amount, small size and/or high dispersion. However, the UV-Vis diffuse reflectance spectra (DRS) show the visible-light absorption of BVNS is greatly extended by the introduction of ZnPc (Figure S2).

The transmission electron microscopy (TEM) image reveals that BVNS is approximately 30-40 nm wide and 50-250 nm long (Figure 1a and Figure S3). Meanwhile, the spacing of lattice fringes is about 0.26 nm, corresponding to the (200) plane of $BiVO_4$. The TEM image of 1ZnPc/BVNS nanocomposite confirms that the BVNS is covered by ZnPc (Figure 1b), and the energy dispersive X-ray (EDX) elemental mapping images unambiguously demonstrate the uniform distribution of Bi, V, O, and Zn elements (Figure S4), indicative of the homogeneous hybridization of ZnPc and BVNS. Besides, the atomic force microscopy (AFM) images and the corresponding height profiles depict the average thicknesses of BVNS and 1ZnPc/$BiVO_4$ are about 7 and 8 nm, respectively (Figure S5), suggesting the increased thickness after coupling ZnPc is about 1nm,[20] which is much favorable for the rapid charge flow in the constructed ultrathin nanocomposite due to the shortened transfer pathway.

To confirm the interfacial bonding mode of BVNS and ZnPc, the peaks of FT-IR spectra of ZnPc (Figure 1c), which assigned to phthalocyanine skeletal and center metal-ligand vibrations, are detected on 1ZnPc/BVNS,[21] further revealing the existence of ZnPc. Importantly, the surface hydroxyl peak intensity of BVNS (at 1630 cm^{-1}) is weakened after ZnPc introduction,[22] indicating ZnPc may connect with the surface hydroxyl groups on BVNS. Also, it is noticed that there is a slight Raman shift along with a gradually strengthened intensity for V-O bonds after ZnPc introduction (Figure 1d).[23-24] Considering the FT-IR spectra, it is suggested that there are well chemical connections and strong interactions between ZnPc and V-O bonds through hydroxyl groups in BVNS. Moreover, the X-ray photoelectron spectra (XPS) indicate the existence of V^{5+} and V^{4+},[25] and the binding energy of V^{4+} has a positive shift after ZnPc introduction. (Figure 1e, Figure S6). Interestingly, the binding energy of Zn is not changed compared with that of pure ZnPc, while there is a positive shift in the N1s binding energy (Figure 1f), indicating ZnPc is connected with BVNS by N in the ligand. Accordingly, it is suggested that the hydroxyl groups on the V-O bonds be linked to the N atoms in the ligand of ZnPc via H-bond interaction.

The first principle periodic DFT simulations further confirm the experimental results of the strong interaction between ZnPc and BVNS after the stable adsorption structure optimization of ZnPc on BVNS surface or hydroxylated BVNS surface via V atoms (Figure 1g-h, Figure S7-S10 and Table S1-S2). The partly hydroxylated BVNS can release adsorption energy of about 0.11 eV to become more stable than the BVNS with -1.14 eV of electronic energy. The average N-H bond length of 1.58 Å and O-H bond length of 2.1 Å are typical weak hydrogen bonding at the interfaces.

The photocatalytic activities of prepared samples for CO_2 reduction were evaluated under visible-light irradiation (λ>420 nm) (Figure 2a). It can be found that all the nanocomposites exhibit higher activities than BVNS, suggesting that the introduction of ZnPc can largely improve the photocatalytic activities for CO_2 reduction. The main product is carbon monoxide and CH_4 is also generated. There is not any other detectable by-product in either liquid or gas phase. Apparently, the 1ZnPc/BVNS delivers the best photocatalytic performance, which improve the BVNS activity by a factor of 4, and a certain amount of oxidation product O_2 is also produced. The quantum efficiencies at the simultaneous light excitation of 520 nm and 660 nm are 4-fold, 10-fold and 16-fold higher than pristine BVNS, $BiVO_4$ nanoflakes (BVNF) and BVNP (Figure 2b, Figure S11 and S12).[11] The optimized photocatalyst also exhibits good stability for 5 cycles in the course of CO_2 conversion (Figure S13). Additionally, the ^{13}C labeled isotope experiment reveals that the reduction products come from CO_2, rather than the decomposition of ZnPc or other residual organics during the synthetic process (Figure S14). In addition, we have also characterised the samples after CO_2 reduction reactions (Figure S15 and Figure S16). The optical absorption and the chemical states of Zn and N for 1ZnPc/BVNS have not changed, further demonstrating the stability of ZnPc during the reactions.

Fluorescence spectra (FS) were measured to explore the charge carrier properties (Figure 2c). A proper amount of ZnPc introduction is favorable for charge separation, however, when the amount of ZnPc is too much, the FS signal starts to decrease, possibly related to the ZnPc aggregation to some extent. The photoelectrochemical and electrochemical impedance spectra further support the FS results (Figure S17 and S18).

To access the mechanism of enhanced charge separation on resulting nanocomposite, the following experiments were designed. According to the energy band alignment of ZnPc and BVNS, a valid Z-scheme photocatalytic system tends to be more reasonable. To prove this, the surface photovoltage spectroscopy (SPS) responses of BVNS and 1ZnPc/BVNS were recorded in N_2 atmosphere (Figure 2d and 2e). There are no detectable SPS

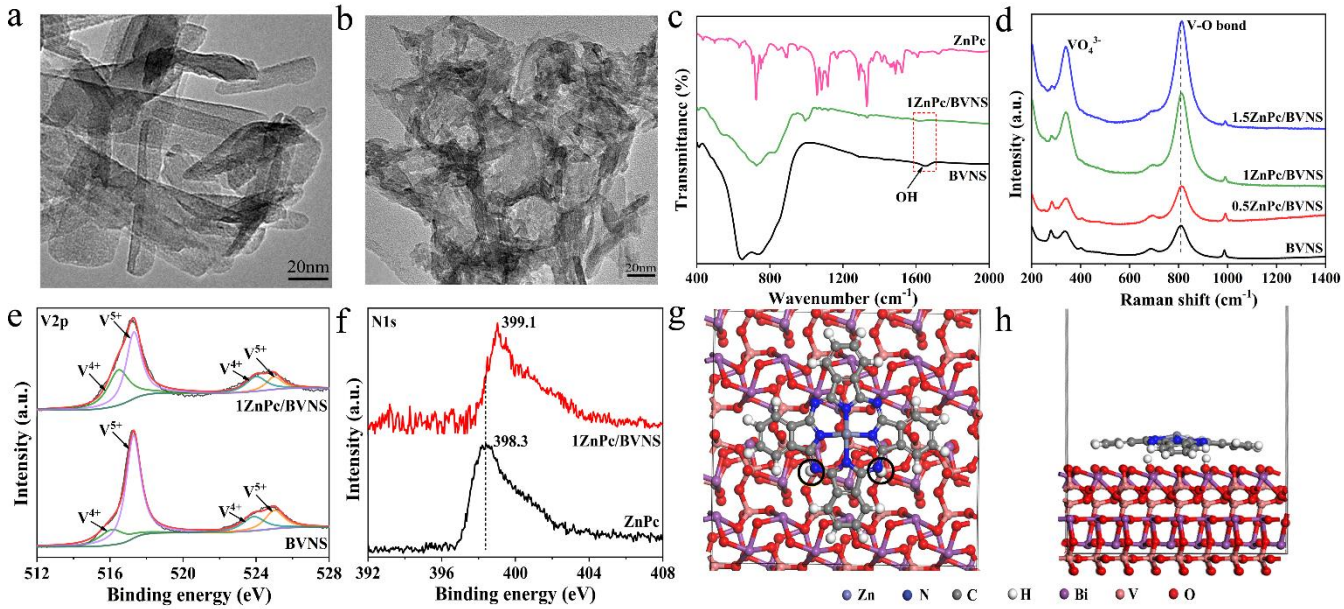

Figure 1. TEM images of BVNS (a), 1ZnPc/BVNS (b), FT-IR spectra of BVNS, 1ZnPc/BVNS and ZnPc (c), Raman spectra of xZnPc/BVNS and BVNS (d), XPS spectra for V2p of 1ZnPc/BVNS and BVNS (e), N1s of ZnPc and 1ZnPc/BVNS (f), DFT optimized ZnPc/BVNS structure and the weak bonding interaction between surface hydroxylated BVNS and ZnPc (black circles) (g, h). x stands for the mass ratio of ZnPc to BVNS.

responses for both of BVNS with and without ZnPc coated, indicating no charge transfer and separation under monochromatic beam probing. This results also eliminate the sensitization dominated by the type II heterojunction. Since there are rather weak SPS signals could be detected between the range of 550 to 750 nm. However, with additional 660 nm monochromatic excitation beam, the nanocomposite exhibits a detectable SPS response in the range of 300-550 nm. As shown in the UV-Vis spectra (Figure S2), coated ZnPc response to the light adsorption between the range of 550 to 750 nm and BVNS adsorb light at wavelength smaller than 550nm. Thus, a charge transfer was only detected by SPS when both of two photocatalysts are excited by excitation and probing beam respectively at the same time. Expectedly, when the sample 1ZnPc/BVNS was exposed to a 520nm monochromatic excitation beam, a SPS response is recorded when probing from 600 to 800 nm. Thus, it is clear that the SPS signals could be detected only if BVNS and ZnPc are excited simultaneously, naturally obeying a Z-scheme charge transfer mechanism. In other words, the photogenerated electrons in the CB of $BiVO_4$ could recombine with the holes in the HOMO of ZnPc so as to greatly enhance the charge separation on the fabricated ZnPc/BVNS nanocomposite.

The proposed Z-scheme mechanism is further confirmed by the monochromatic photocurrent action spectra (Figure 2f). The photocurrent density of BVNS gradually increases as the excitation wavelength decreases from 520 to 400 nm. For ZnPc, it evenly increases from 700 to 600 nm, consistent with its specific absorption. Noticeably, the photocurrent density of 1ZnPc/BVNS obeys the similar law with pure BVNS and ZnPc on the corresponding excitation wavelengths. In this case, there is weak or no charge transfer and separation due to the single excitation of BVNS or ZnPc. However, when 660 nm monochromatic light is assisted to excite ZnPc, the photocurrent density of 1ZnPc/BVNS sharply increases from 520 to 400 nm. In particular, the recorded photocurrent density is much larger

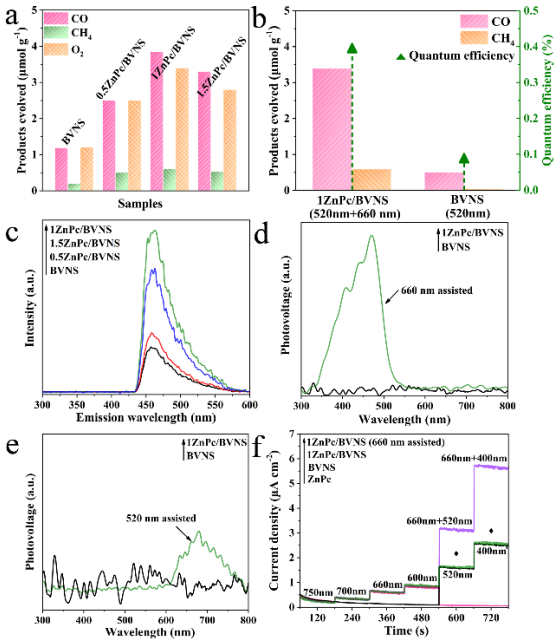

Figure 2. Photocatalytic activities for CO_2 conversion under visible-light irradiation for 4 h of xZnPc /BVNS and BVNS (a), photocatalytic activities for CO_2 conversion and the corresponding QE under monochromatic beams (at 520 and 660 nm) for 1ZnPc/BVNS and 520 nm for BVNS (b), fluorescence spectra related to the formed hydroxyl radicals of BVNS and xZnPc/BVNS (c), SPS responses of 1ZnPc/BVNS and BVNS in N_2 atmosphere assisted with 660 nm (d) and 520 nm monochromatic beam (e), normalized photocurrent action spectra of BVNS, ZnPc and 1ZnPc/BVNS under different monochromatic light irradiation (f). The marks in Figure 2f stand for the sum of current densities of BVNS and ZnPc under 520 nm and 660 nm monochromatic irradiation.

than that of the sum of individual BVNS and ZnPc. This result is ascribed to the Z-scheme mechanism on the photo-induced charge transfer and separation, and it is also supported by the well-designed FS spectra (Figure S19). Considering the individual optical absorption ability of each constituent in the complex, we have also balanced the intensity of the two specific exciting lights (Figure S20). It is clear that there is an optimized light intensity for exciting BVNS and ZnPc, further declaring the importance of light absorption matching between these two constituents in Z-scheme system.

Subsequently, the low-temperature electron paramagnetic resonance (EPR) technique was employed to explore the process of electron transfer from ligand to central coordinated Zn^{2+}. A peak assigned to V^{4+} ($3d^1$) was detected on BVNS in dark (Figure S21a),[26] supporting the XPS results. The typical EPR signals of ZnPc centering at g=1.9998 and 1.9684 (Figure S21b), resulting from the dissociative free electrons in the ZnPc ligand and the partially reduced Zn^+, are observed, respectively.[27] Interestingly, there is no detectable change of EPR signals under 520 or 660 nm excitation (Figure S22a and S22b). However, the intensity is weakened when both BVNS and ZnPc are excited at the same time (Figure 3a). This is due to the electrons of BVNS transfer to the ZnPc, and the electron configuration of partial V^{4+} is changed from $3d^1$ to $3d^0$, leading to the decreased electronic spin signal. This gives a strong evidence for the Z-scheme charge transfer between BVNS and ZnPc.

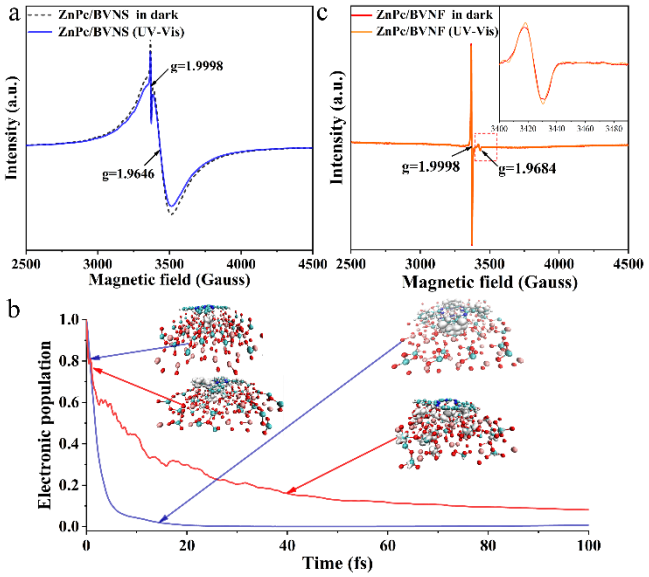

Figure 3. EPR spectra of ZnPc/BVNS with UV-Vis light irradiation at 98K (a), the time dependent survival probability (TDSP) curves of the excited electrons transfer between partly hydroxylated BVNS and ZnPc during the injection process (b) (Red: from ZnPc to BVNS; Blue: from BVNS to ZnPc), and EPR spectra of ZnPc/BVNF with UV-Vis light irradiation at 98K (c) with the enlarged in the insert.

Moreover, the excited state interfacial electron transfer process is also evidenced fundamentally. It can be seen from Figure 3b that the charge transfer at the interface is basically completed within 100 fs. In addition, the charge transfer between ZnPc and BVNS is a competitive process both forward and reverse directions, but the transfer from BVNS to ZnPc is dominant, which is faster than the reverse charge transfer (10 fs Vs 80 fs for 80% population).

Notably, if the electrons could further transfer to the central Zn^{2+}, there would be a variation for EPR signal of Zn^+. However, it is hard for the Zn^+ signal (g=1.9684) to distinguish due to its rather weak intensity and the similar g factor to V^{4+} in ZnPc/BVNS. Thus, BVNF was used to prepare a similar nanojunction to preclude the strong impact of V^{4+}, owing to its discriminative g factor of 2.0260 that results from the oxygen vacancy.[28] Similarly, no detectable change of Zn^+ signal is observed under 520 or 660 nm excitation for ZnPc/BVNF (Figure S23). Impressively, the intensity of Zn^+ signal is strengthened after ZnPc and BVNF are excited simultaneously (Figure 3c), suggesting that the electron transfer from the ligand to the central metal takes place based on the confirmed Z-scheme charge transfer.

Furthermore, electrochemical reduction measurements were also conducted to verify the catalytic function of the coordinated central metal sites, and the phthalocyanine-coupled BVNS (H_2Pc/BVNS) was synthesized to take as a reference (Figure S24). H_2Pc/BVNS exhibits a similar onset potential compared with that of BVNS, and as expected, it is much lower for ZnPc-coupled one, indicating that the ZnPc is more favorable for H_2O reduction due to the catalytic effect of zinc ions. By comparison, the reduction behavior of CO_2 is also much preferred, and this result is consistent with CO_2 TPD curves (Figure S25). Since the large π network of ZnPc is highly favorable for adsorption of CO_2 molecules through π-π interactions,[29] ZnPc/BVNS presents a much larger adsorption amount of CO_2 molecules than those on the pristine BVNS. Meanwhile, it is noticed that both H_2Pc and ZnPc introduction are beneficial to improve the photocatalytic activity for CO_2 reduction, although ZnPc-coupled one has better performance (Figure S26a). Interestingly, it is verified by the SPS responses and FS results that the enhanced charge separation on H_2Pc/BVNS and ZnPc/BVNS is roughly same (Figures S26b and 26c), indicating the important role of central metal in the catalysis to CO_2 reduction, rather than in the charge separation.

Accordingly, a new Z-scheme schematic of photogenerated charge carrier transfer and separation on ZnPc/BVNS is proposed (Scheme 2). When both BVNS and ZnPc are excited simultaneously under visible-light irradiation, the photogenerated electrons in the CB of BVNS would quickly combine with the photoinduced holes in the HOMO of ZnPc owing to their close band edge positions. In this case, the spatially separated holes on BVNS and electrons on ZnPc would possess thermodynamically sufficient energy to induce redox reactions, consequently leading to the promoted charge separation and hence to the improved photocatalytic activities. Moreover, the central metal cation Zn^{2+} could accept the separated electrons from the ligand and then provide the catalytic function for CO_2 reduction.

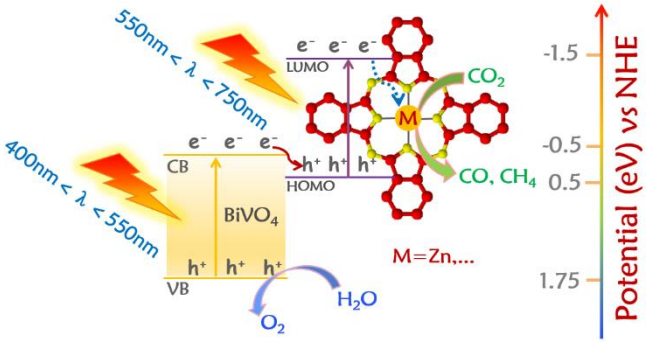

Scheme 2. Proposed Cascade Z-scheme mechanism of photogenerated charge transfer on MPc-coupled BVNS (M represents transition metal).

Significantly, the proposed new Z-scheme charge transfer strategy is not limited to ZnPc/BVNS system, it is also feasible for FePc and CoPc-coupled ones, though ZnPc/BVNS exhibits the highest charge separation and the best photocatalytic activity for CO_2 conversion (Figure S27a and 27b). This is attributed to its preferable catalytic function and CO_2 adsorption capacity (Figure S28 and S29). In addition, the scanning Kelvin probe implies the band edge position of ZnPc is much well matching with BVNS due to the p-type character of MPc (Figure S30 and S31), and the electron transfer from BVNS to ZnPc is more accessible, which is more suitable for the Z-scheme charge transfer rule.

In summary, the well-designed ZnPc/BVNS ultrathin nanocomposite exhibits excellent visible-light photocatalytic activities for CO_2 conversion, thanks to a novel Z-scheme charge transfer mechanism. The remarkable activities are attributed to both of the enhanced charge separation and the extended visible light absorption. Meanwhile, it is evidenced that the transferred electrons from ligand to central metal cation empower the catalytic function of Zn^{2+} for CO_2 reduction. Similarly, the photocatalytic activities of BVNS could be also improved after coupling with other MPc. Among fabricated MPc/BVNS nanocomposites, the ZnPc/BNVS exhibits the optimal activity for CO_2 reduction, resulting into 16 times higher quantum yield for CO_2 conversion than the counterpart $BiVO_4$ nanoparticles, which is attributed to the synergistic effects of the better charge separation and preferable catalytic role of central metal cation. Accordingly, this work not only develops a facile strategy for wide-visible-light responsive $BiVO_4$-based photocatalytic nanomaterials, but also opens up a new route for a cascade Z-scheme photocatalytic system on efficient solar fuel production.

Acknowledgements

L.Q. J, J. B, Z.Q. Z and Y. Q acknowledge financial support from the NSFC project (U1805255, 21501052 and 91622119), the Program for Innovative Research Team in Chinese Universities (IRT1237), the and UNPYSCT-2016173. J. X. and J. T. are thankful to the UK EPSRC (EP/N009533/1), Royal Society Newton Advanced Fellowship grant (NAF\R1\191163) and Leverhulme Trust (RPG-2017-122).

Keywords: $BiVO_4$ nanosheet • CO_2 conversion • Metal phthalocyanine/$BiVO_4$ nanocomposite • Novel Z-scheme • Wide-visible-light catalysis

[1] L. Collado, A. Reynal, F. Fresno, M. Barawi, C. Escudero, V. Perez-Dieste, J. M. Coronado, D. P. Serrano, J. R. Durrant, V. A. de la Pena O'Shea, *Nat. Commun.* **2018,** *9*, 4986.
[2] P. Zhang, S. B. Wang, B. Y. Guan, X. W. Lou, *Energy Environ. Sci.* **2019**, *12*, 164.
[3] H. L. Tan, R. Amal, Y. H. Ng, *J. Mater. Chem. A* **2017**, *5*, 16498.
[4] H. L. Tan, X. M. Wen, R. Amal, Y. H. Ng, *J. Phys. Chem. Lett*. **2016**, *7*, 1400.
[5] H. L. Tan, H. A. Tahini, X. M. Wen, R. J. Wong, X. Tan, A. Iwase, A. Kudo, R. Amal, S. C. Smith, Y. H. Ng, *Small* **2016**, *12*, 5295.
[6] M. Zhu, Z. Sun, M. Fujitsuka, T. Majima, *Angew. Chem. Int. Ed.* **2018,** *57*, 1.
[7] S. Wang, P. Chen, Y. Bai, J. H. Yun, G. Liu, L. Z. Wang, *Adv. Mater.* **2018,** *30*, 1800486.
[8] S. Gao, Y. Lin, X. Jiao, Y. Sun, Q. Luo, W. Zhang, D. Li, J. Yang, Y. Xie, *Nature* **2016,** *529*, 68.
[9] S. Gao, B. C. Gu, X. C. Jiao, Y. F. Sun, X. L. Zu, F. Yang, W. G. Zhu, C. M. Wang, Z. M. Feng, B. J. Ye, Y. Xie, *J. Am. Chem. Soc.* **2017,** *139*, 3438.
[10] M. Xie, X. Fu, L. Q. Jing, P. Luan, Y. J. Feng, H. G. Fu, *Adv. Energy Mater.* **2014,** *4*, 1300995.
[11] a) J. Bian, Y. Qu, X. Zhang, N. Sun, D. Tang, L. Q. Jing, *J. Mater. Chem. A* **2018,** *6*, 11838; b) S.J.A. Moniz, J. Tang, *ChemCatChem,* **2015**, 7(11), 1659.
[12] C. Kim, K. M. Cho, A. Al-Saggaf, I. Gereige, H. T. Jung, *ACS Catal.* **2018,** *8*, 4170.
[13] Q. Yuan, D. Liu, N. Zhang, W. Ye, H. Ju, L. Shi, R. Long, J. Zhu, Y. Xiong, *Angew. Chem. Int. Ed.* **2017,** *56*, 4206.
[14] D. J. Martin, P. J. T. Reardon, S. J. A. Moniz, J. Tang, *J. Am. Chem. Soc.* **2014,** *136*, 12568.
[15] Y. Wang, G. Tan, T. Liu, Y. Su, H. Ren, X. Zhang, A. Xia, L. Lv, Y. Liu, *Appl. Catal. B-Environ.* **2018,** *234*, 37.
[16] A. Tiwari, N. V. Krishna, L. Giribabu, U. Pal, *J. Phys. Chem. C* **2018,** *122*, 495.
[17] X. Zhang, T. Peng, L. Yu, R. Li, Q. Li, Z. Li, *ACS Catal.* **2015,** *5*, 504.
[18] X. Zhang, L. Yu, C. Zhuang, T. Peng, R. Li, X. Li, *ACS Catal.* **2014,** *4*, 162.
[19] S. Mori, M. Nagata, Y. Nakahata, K. Yasuta, R. Goto, M. Kimura, M. Taya, *J. Am. Chem. Soc.* **2010,** *132*, 4054.
[20] L. M. Arellano, L. Martin-Gomis, H. B. Gobeze, D. Molina, C. Hermosa, M. J. Gomez-Escalonilla, J. L. G. Fierro, A. Sastre-Santos, F. D'Souza, F. Langa, *Nanoscale* **2018,** *10*, 5205.
[21] M. Zhang, C. Shao, Z. Guo, Z. Zhang, J. Mu, T. Cao, Y. Liu, *ACS Appl. Mater. Interfaces* **2011,** *3*, 369.
[22] Y. Luan, L. Jing, M. Xie, X. Shi, X. Fan, Y. Feng, *Phys. Chem. Chem. Phys.* **2012,** *14*, 1352.
[23] Y. Zhang, H. Gong, Y. Zhang, K. Liu, H. Cao, H. Yan, J. Zhu, *Eur. J. Inorg. Chem.* **2017,** 23, 2990.
[24] J. Q. Yu, A. Kudo, *Adv. Funct. Mater.* **2006,** *16*, 2163.
[25] F. Xiao, X. Song, Z. Li, H. Zhang, L. Zhang, G. Lei, Q. Xiao, Z. Hu, Y. Ding, *J. Mater. Chem. A* **2017,** *5*, 17432.
[26] V. I. Merupo, S. Velumani, K. Ordon, N. Errien, J. Szaded, A. H. Kassiba, *CrystEngComm.* **2015,** *17*, 3366.
[27] S. Repp, S. Weber, E. Erdem, *J. Phys. Chem. C* **2016,** *120*, 25124.
[28] J. Xu, Z. Bian, X. Xin, A. Chen, H. Wang, *Chem. Eng. J.* **2018,** *337*, 684.
[29] Z. Sun, N. Talreja, H. Tao, J. Texter, M. Muhler, J. Strunk, J. Chen, *Angew. Chem. Int. Ed.* **2018,** *57*, 7610.

Dimension-matched zinc phthalocyanine/$BiVO_4$ nanosheet (ZnPc/BVNS) nanocomposites as efficient wide-visible-light-driven photocatalysts for converting CO_2 to CO and CH_4.

J. Bian, J. N. Feng, Z. Q. Zhang, Z. J. Li, Y. H. Zhang, Y. D. Liu, S. Ali, Y. Qu, L. L. Bai, F. Q. Bai, J. J. Xie, D. Y. Tang, X. Li, J. W. Tang*, L. Q. Jing**

Page No. – Page No.

Dimension-matched Zinc Phthalocyanine/$BiVO_4$ ultrathin nanocomposites for CO_2 Reduction as Efficient Wide-Visible-Light-Driven Photocatalysts via a Cascade Charge Transfer